Carbohydrate Polymers 227 (2020) 115338

Contents lists available at ScienceDirect

Carbohydrate Polymers

journal homepage: www.elsevier.com/locate/carbpol

Biocompatible AIE material from natural resources: Chitosan and its multifunctional applications

Zhenzhen Dong[a], Hanrui Cui[a], Yandong Wang[a], Chunlei Wang[a], Yan Li[b,c,*], Caiqi Wang[a,*]

[a] School of Chemical Sciences, University of Chinese Academy of Sciences, Beijing 100049, China
[b] School of Materials Science and Engineering, Beihang University, Beijing 100191, China
[c] Beijing Advanced Innovation Centre for Biomedical Engineering, Beihang University, Beijing 100191, China

ARTICLE INFO

Keywords:
Aggregation-induced emission
Chitosan
Multifunctional applications

ABSTRACT

New sources of AIE materials with good water solubility, biocompatibility, degradability, and mass production are urgently needed. Here, we found that chitosan, a very abundant polysaccharide in nature, has fluorescence emission in both solid and solution states with AIE effect, and explored its multifunctional applications. Chitosan can emit a variety of colors from blue to red at different excitation wavelengths with excellent multicolor imaging capabilities at the cellular level. Utilizing the cationic and antibacterial properties of chitosan, the quantification of bacteria can be achieved through the AIE effect. Concurrently, it can be used as fluorescent probes for multi-channel bacterial imaging via lighting-up bacteria. Furthermore, the chitosan solution exhibits a sensitive quenching response to Fe^{3+}, which can be used as a biosensor for detecting the concentration of Fe^{3+}. These interesting results indicate that chitosan will have broad application prospects as a new class of AIE material.

1. Introduction

Fluorescent materials are widely used because of their excellent properties including sensitivity, in-situ operability, non-invasiveness and high spatial-temporal resolution. (Zhu & Yang, 2013; Lin et al., 2014; Sun et al., 2015; Yan et al., 2016). However, when most conventional organic dyes are used at a high concentration or in aggregation state, their fluorescence signal is significantly weakened or even disappears due to intermolecular π-π stacking. This is well-known as aggregation-caused quenching (ACQ) effect (Qin et al., 2012; Liang et al., 2015; Tian et al., 2016). Different from traditional ACQ materials, aggregation-induced emission (AIE) materials do not emit light or emit weak light at low concentrations, but emit very strong fluorescence upon aggregation (Mei et al., 2014; Mei et al., 2015; Cao et al., 2017a, 2017b; Huang et al., 2018; Zheng et al., 2019). Due to these unique photophysical properties and their potential applications in biomedicine, optoelectronic devices, and chemical sensing, more and more researchers are paying attention to AIE materials (Wang et al., 2016; Cheng et al., 2017; Jiang et al., 2018; Li et al., 2018; Song et al., 2018; Tian et al., 2019).

The current research on the AIE effect has been very in-depth (Cheng et al., 2017; Huang et al., 2017; Jiang, Liu, Liu, et al., 2017; Jiang, Gu, et al., 2018). For example, Jiang, Gu, et al. (2018) reported three AIE molecules based on diphenyl isoquinolinium derivatives. They have high structural stability, two-photon absorption and tunable color. Cheng et al. (2017) designed two cationic AIE-active tetraphenylethene (TPE) derivatives for humidity detection. However, most of the sources of AIE materials are organically synthesized (Gu et al., 2018). Although these AIE materials offer structural diversity and color tunability, their disadvantages are also obvious: complex synthesis, high cost, environmental toxicity, poor degradation, and poor biocompatibility, which will limit their practical applications to some extent (Shen et al., 2016; Shi et al., 2017; Chen, Zhang, et al., 2018; Wang et al., 2018). Furthermore, traditional AIE materials, such as TPE, are mostly non-planar conjugated molecular conformations with poor water solubility, which limits in vivo studies. Therefore, new sources of AIE materials are needed with good water solubility, biocompatibility, degradability, and mass production.

Nature is a rich treasure house, which provides us with inexhaustible resources for food, clothing, shelter, and transportation. Polysaccharides, such as starch, cellulose, and chitosan (CS), as the most abundant biological macromolecules in nature, exist in almost all living things. They have been extensively studied in the applications of industrial materials and biomedicine, but their fluorescent properties have received little attention (Liu et al., 2009; Olsson et al., 2010; LogithKumar et al., 2016; Yu et al., 2018). Recently, Dou et al. (2018)

* Corresponding authors.
E-mail addresses: liyan@buaa.edu.cn (Y. Li), wang-caiqi@ucas.ac.cn (C. Wang).

https://doi.org/10.1016/j.carbpol.2019.115338
Received 18 June 2019; Received in revised form 11 September 2019; Accepted 15 September 2019
Available online 16 September 2019
0144-8617/

studied the fluorescence behavior of sodium alginate and proposed a clustering-triggered emission (CTE) mechanism. Due to the abundance, versatility, and excellent biocompatibility of biomacromolecules, exploring their fluorescence properties will help develop a new generation of diagnostic and sensing materials.

Chitosan, a very abundant polysaccharide in nature, is obtained via the deacetylation of chitin. It is a bioactive polymer with antibacterial activity, non-toxicity, easy modification, and biodegradation, which makes it widely used in medicine, food, water treatment and other fields (Kumar, 2000; Kumar et al., 2004; Rinaudo, 2006; Hou et al., 2017). For the fluorescence study of chitosan, it mainly focuses on two aspects: modifying the fluorescent group (Wang et al., 2013; Wang et al., 2016); crosslinking of chitosan and aldehyde compounds (Wei et al., 2007; Wei et al., 2008; Wang et al., 2014; Song, Zhou, et al., 2018). For example, Wang et al. (2016) modified TPE on chitosan for visualization of the gelation process. Wei et al. (2007) prepared uniform size self-fluorescent chitosan microspheres crosslinked with glutaraldehyde through membrane emulsification technique. The n-π^* transition of the C=N bond in the Schiff base formed during the crosslinking reaction causes auto-fluorescence of the chitosan cross-linking product. However, the AIE effect of chitosan in its native form without chemical modification has not been reported. Therefore, this work deeply studied the AIE effect of chitosan with different molecular weights. Combining the excellent biocompatibility and antibacterial property of chitosan, as well as the application of traditional AIE materials, we intend to explore its applications in cell and bacterial imaging, bacteria detection, and metal ion concentration detection. Chitosan as a new class of AIE material will provide a wide range of practical applications.

2. Experimental section

2.1. Materials

Chitosan (CS-1, $M_W \approx 3 \times 10^3$, degree of acetylation (DA) = 6.5%, Shanghai Yuanye), chitosan (CS-2, $M_W \approx 3 \times 10^4$, DA = 8.8%, Shanghai Macklin), chitosan (CS-3, $M_W \approx 4 \times 10^5$, DA = 3.6%, Beijing Henghuibio), chitosan (CS-4, $M_W \approx 4 \times 10^5$, DA = 9.1%, Beijing Henghuibio), and ferric trichloride (99%, Beijing Sinopharm) were used upon arrival. The MCF-7 cell lines were obtained from Chinese Academy of Medical Sciences. The bacterial strains of *Escherichia coli* (*E. coli*) ATCC25922 was obtained from American Type Culture Collection.

2.2. Characterizations

Fourier transform infrared (FTIR) spectra were obtained on Bruker TENSOR II IR spectrometer. The ^{1}H nuclear magnetic resonance (NMR) spectra were recorded on a JEOL JNM-ECZS400. Fluorescence measurements were carried on HORIBA FluoroMax-4 spectrofluorometer. Samples of different concentrations were dissolved in water or 1% aqueous acetic acid solution. The UV–vis absorbance was achieved on Shimadzu UV-2500. The fluorescence lifetime and quantum yield were obtained on Edinburgh FLS1000 equipped with an integrating sphere. Dynamic light scattering (DLS) spectra were achieved on Malvern Nano ZS. Fluorescence microscope images were obtained on Leica DM6000B. Cell imaging and bacterial imaging were observed by confocal laser scanning microscopy (CLSM, Zeiss LSM880).

2.3. Cytotoxicity assessment

The cytotoxicity of CS was determined by MTT assay using MCF-7 cells. Briefly, cells were cultured in 96-well plates and incubated in Dulbecco's Modified Eagle Medium (DMEM) supplemented with 10% fetal bovine serum (FBS) for 1 d. The cell density per well is 3000. Then, the medium containing the samples of different concentrations was added and cultured for another 1 d. After removing the medium, 10 μL MTT and 90 μL DMEM were added and cultured for another 4 h. Finally, the crystals (formazan) were dissolved by DMSO, and the absorbance was measured at 570 nm. The cell viability was defined as a ratio of the absorbance of experimental group and control group.

2.4. Cell imaging

MCF-7 cells were cultured onto a glass dish for 24 h in DMEM supplemented with 10% FBS. CS-1 was dissolved in the medium, resulting in a final concentration of 100 μg mL^{-1}. After incubating the cells for 3 h using the mixtures described above, the medium was removed. The cells were washed three times with PBS and then fixed with 4% paraformaldehyde. MCF-7 cells were observed by CLSM, and CS-1 was excited at 405, 488, and 561 nm, respectively. Fluorescence emission was received at 410–501, 493–622, and 566–685 nm.

2.5. Bacterial culture and concentration detection

A single colony of *E. coli* were transferred to LB liquid medium and cultured overnight at 37 °C. The bacteria were harvested by centrifugation at 5000 rpm (2650 g) for 10 min and resuspended in the water. Different concentrations of the bacterial suspension were mixed in an equal volume with a 100 μg mL^{-1} CS-1 aqueous solution to obtain a predetermined bacterial concentration. After 12 h of gentle vibration, the fluorescence spectra were measured at room temperature.

2.6. Bacterial imaging

E. coli was harvested by centrifugation at 5000 rpm (2650 g) for 10 min and resuspended in water. Then bacterial suspension was mixed with the CS-1 aqueous solution such that the final concentration of CS-1 was 150 μg mL^{-1}. The washed bacteria were observed by CLSM, and CS-1 was excited at 405, 488, and 561 nm, respectively. The fluorescence emission was received in the range of 410–501, 493–622, and 566–685 nm.

2.7. Detection of Fe^{3+}

Ferric chloride was used as a source of Fe^{3+}. A series of concentration gradient of Fe^{3+} aqueous solution was configured. Then, different concentrations of the Fe^{3+} aqueous solution was mixed in an equal volume with a 1 mg mL^{-1} CS-1 aqueous solution to obtain a predetermined Fe^{3+} concentration. After 12 h of gentle vibration, the fluorescence spectra were measured at room temperature.

2.8. Statistical analysis

All experimental data were performed in triplicate and the results were presented as the average.

3. Results and discussion

3.1. AIE effect

Chitosan is commercial product with very mature processes. The different molecular weights chitosan (CS-1; CS-2; CS-3; CS-4) used in this work were all commercially available and their purity had been verified by FTIR spectra and NMR spectra (**Figs. S1-S4**). The solid powders of CS-1, CS-2, CS-3 and CS-4 emitted pale blue light under 365-nm UV illumination, indicating that chitosan had solid-state emission (Fig. 1A). Since chitosan with high molecular weights was insoluble in neutral aqueous solution, the AIE effect was studied by the photoluminescence behavior of CS-1, CS-2, CS-3, and CS-4 in 1% aqueous acetic acid solution. Taking CS-1 as an example, excited at λ_{ex} = 360 nm, it exhibited a very strong fluorescence emission, and the emission peak appeared at around 435 nm (Fig. 1B). In addition, the

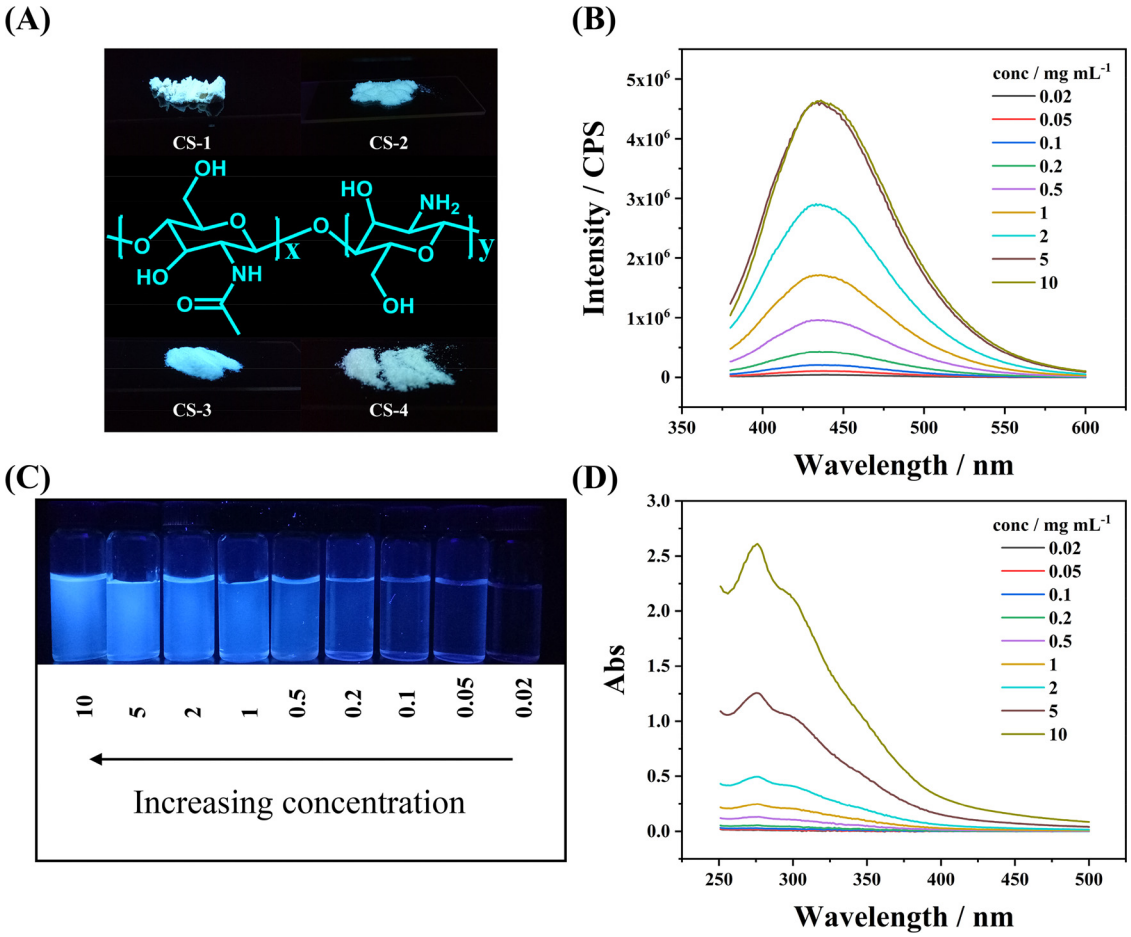

Fig. 1. (A) Fluorescence photographs of CS powders under 365 nm ultraviolet light. (B) Fluorescence spectra of CS-1 with various concentrations excited by 360 nm (slit width: 3 nm). (C) Fluorescence photograph of different concentrations of CS-1 under 365 nm ultraviolet light. (D) UV–vis absorption spectra of CS-1 with various concentrations.

fluorescence intensity of CS-1 continuously increased with increasing concentration, exhibiting an AIE effect. A similar phenomenon was seen from the photograph under 365-nm UV light. (Fig. 1C). The UV–vis absorption of CS-1 was weak at low concentrations (Fig. 1D). Its absorption gradually increased with increasing concentration, and two shoulder peaks were observed at 276 nm and 303 nm. The edge of the absorption spectrum gradually shifted to higher wavelengths as the concentration increased, which may explain that the fluorescence enhancement was not apparent due to energy transfer when the concentration exceeded 5 mg mL^{-1} (Chen, Luo, et al., 2018). The CS-2, CS-3, and CS-4 also had an AIE effect, and their fluorescence and absorption spectra were measured (**Figs. S5-S7**). The fluorescence lifetime and quantum yield of CS-1, CS-2, CS-3, and CS-4 appeared to be irregular and there was a phenomenon that sometimes they were lower in a solid state (**Table S1**). This may be because they were sourced from different manufacturers and had self-absorption or exciton coupling (Chen, Luo, et al., 2018). In addition, the fluorescence intensity of CS was only slightly reduced after continuous irradiation with 365 nm ultraviolet light for 30 min in 1% aqueous acetic acid solution (**Fig. S8**). This indicates that chitosan has good photostability (Liu et al., 2017; Tian et al., 2017). It can be seen from the dynamic light scattering spectra that CS forms nano-aggregates in 1% aqueous acetic acid solution (**Fig. S9**).

3.2. Excitation-dependent fluorescence

Chitosan showed obvious excitation-dependent fluorescence and could emit a variety of colors from blue to red at different excitation wavelengths. Taking CS-1 as an example, the fluorescence emission of the solution was red-shifted with increasing excitation wavelength, and the optimal excitation wavelength was 360 nm (Fig. 2A). The fluorescence emission weakened continuously when the excitation wavelength exceeded 360 nm. Interestingly, this phenomenon is often seen in the fluorescence properties of luminescent polymers containing unconventional chromophores (Yang & Pan, 2009; Shang et al., 2017; Chen, Luo, et al., 2018), quantum dots (Hasan et al., 2018), and carbon dots (Tao et al., 2018). The CS-1 solid powder emitted blue, green, and red fluorescence when excited by ultraviolet light (340–380 nm), blue light (460–500 nm), and green light (540–552 nm), respectively (Fig. 2B). Similarly, CS-2, CS-3, and CS-4 also exhibited excitation-dependent fluorescence (Fig. 2**C-2H**). Combined with experimental data and related literature (Yang & Pan, 2009; Yang et al., 2011), this excitation-dependent fluorescence of CS may be related to its broader molecular weight distribution. The use of this property of CS is promising for multi-channel bioimaging, enabling more accurate localization of markers.

3.3. Fluorescence mechanism

Luminescent macromolecules are generally constructed by π-aromatic building blocks functioning as emitting units. Recently, other types of macromolecules containing only the auxochrome (aliphatic amines, carbonyl groups, ester groups and amides) have been shown to emit fluorescence under appropriate conditions and exhibit an AIE effect (Chen, He, et al., 2018; Dou et al., 2018; Zhao et al., 2018; Dong et al., 2019; Tomalia et al., 2019). For the explanation of the emission

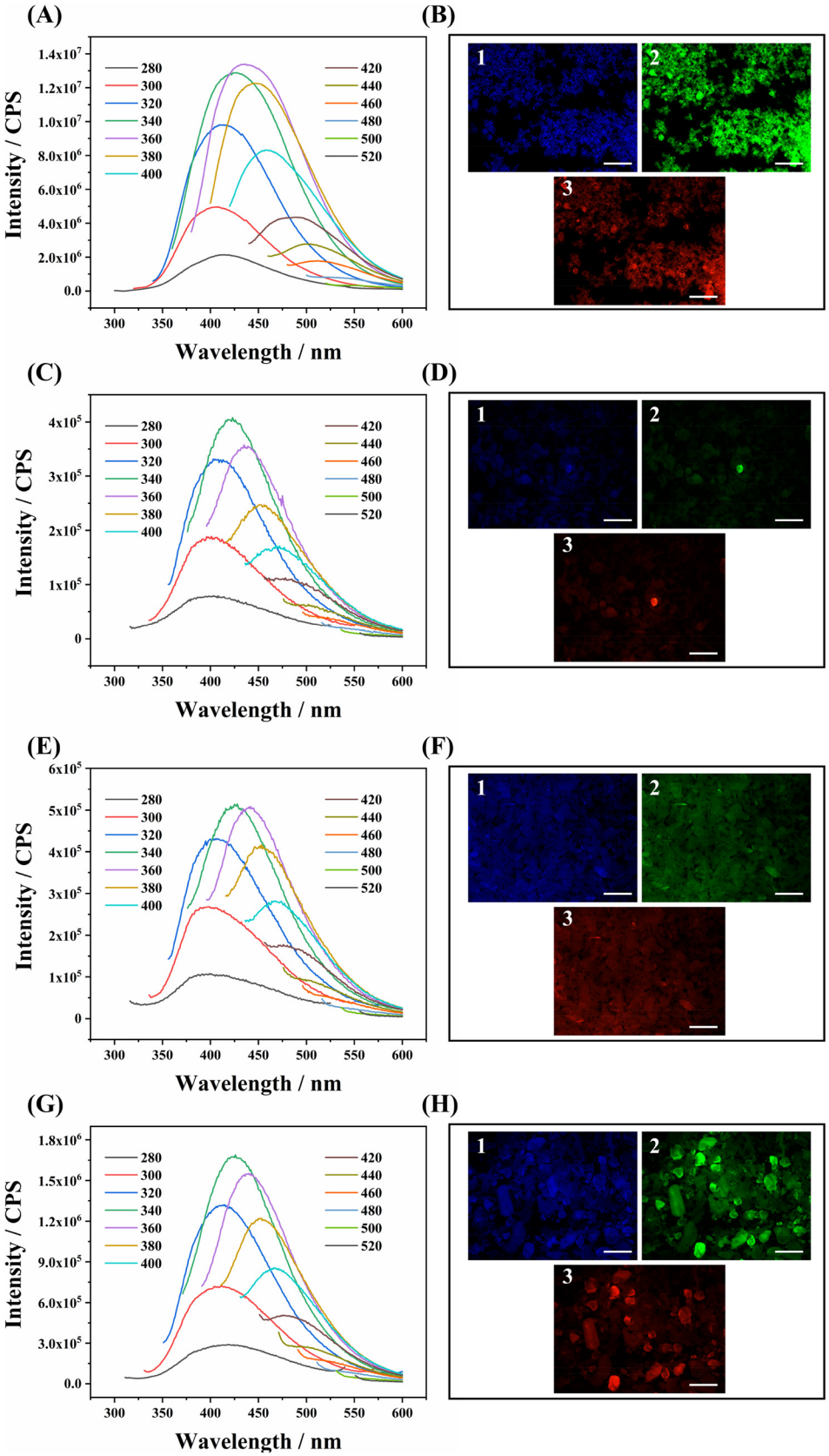

Fig. 2. Fluorescence spectra of CS-1 (A), CS-2 (C), CS-3 (E), and CS-4 (G) solution (1 mg mL^{-1}) with different excitation wavelengths (slit width: 5 nm). Fluorescence microscope images of CS-1 (B), CS-2 (D), CS-3 (F), and CS-4 (H) solid powder. 1, 2, and 3 refer to images taken under UV (340–380), blue (460–500), and green (540–552) lights, respectively (Scale bar 500 μm).

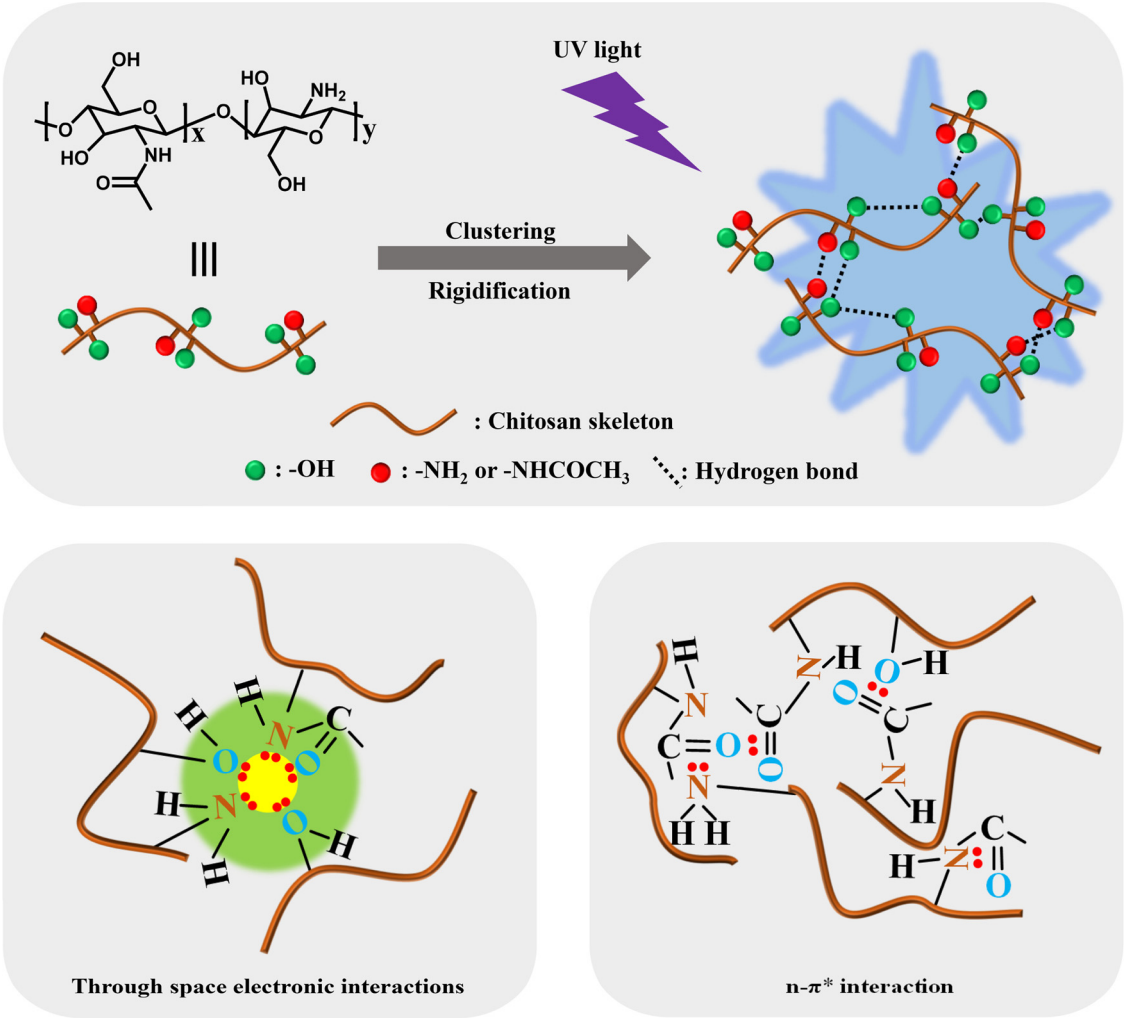

Fig. 3. Schematic illustration of emission mechanism of CS.

mechanism of such substances, the Yuan group proposed a CTE effect (Chen, He, et al., 2018; Chen, Luo, et al., 2018; Dou et al., 2018). The clustering of unconventional chromophores with π and lone-paired (n) electrons and subsequent electron cloud overlap together with simultaneous conformation rigidification are the causes of intrinsic light emission. The above results have shown that solution and solid states of different molecular weights chitosan can emit fluorescence, which can also be explained by the CTE effect (Fig. 3). The clustering of hydroxyl, amino and acetylamino groups in chitosan can provide an effective through space intramolecular and intermolecular interactions among them and a rigid conformation simultaneously. Thus, extended electron delocalization is formed which can be excited to produce a radiation emission. On the other hand, there are a large number of hydrogen bonds in chitosan, which not only rigidify the molecular conformation, but also promote the through space conjugation among adjacent n and π electrons, further enhancing the fluorescence emission. CS-3 and CS-4 have the same molecular weight, but CS-4 has a stronger fluorescence emission (**Fig. S10**). It is certainly related to the local molecular structure. Even though two different commercial chitosan have the same molecular weight and degree of acetylation, they may have different microstructures (distribution of acetylamino along the chains).

3.4. Multifunctional applications

Chitosan is widely used due to its environmental friendliness, biocompatibility, biodegradability, and ease of use (Rinaudo, 2006). The discovery of the AIE effect of chitosan will lay the foundation for diverse applications.

3.4.1. Cell imaging

Considering the excellent biocompatibility and AIE effect of chitosan, we studied the capacity for cell imaging by taking water-soluble CS-1 as an example. First, the cytotoxicity of different concentrations of CS-1 on MCF-7 cells was determined by MTT assay. When the concentration was increased to 1 mg mL^{-1}, the cell viability remained above 90%, indicating that the chitosan used here had excellent biocompatibility (**Fig. S11**). The cell imaging behavior of CS-1 was investigated next via CLSM using MCF-7 cells. Since CS-1 exhibited excitation-dependent fluorescence, after co-incubation with cells for 3 h, images of CLSM were acquired by using three separate channels to collect emission of blue, green, and red channels. Blue fluorescence emission appeared in the cells when excited by a 405 nm-laser (Fig. 4). When excited with 488 and 561 nm lasers, green and red fluorescence emission was observed in the cells, respectively. These results indicate that chitosan can be rapidly internalized by cells and has good multicolor cell imaging ability. At the same time, this multi-channel imaging can locate cells more accurately. In addition, compared with the traditional AIE materials, low molecular weight chitosan has the advantages of good water solubility, biocompatibility, degradability, and mass production, which will have great potential application value for biomedical research and clinical diagnosis.

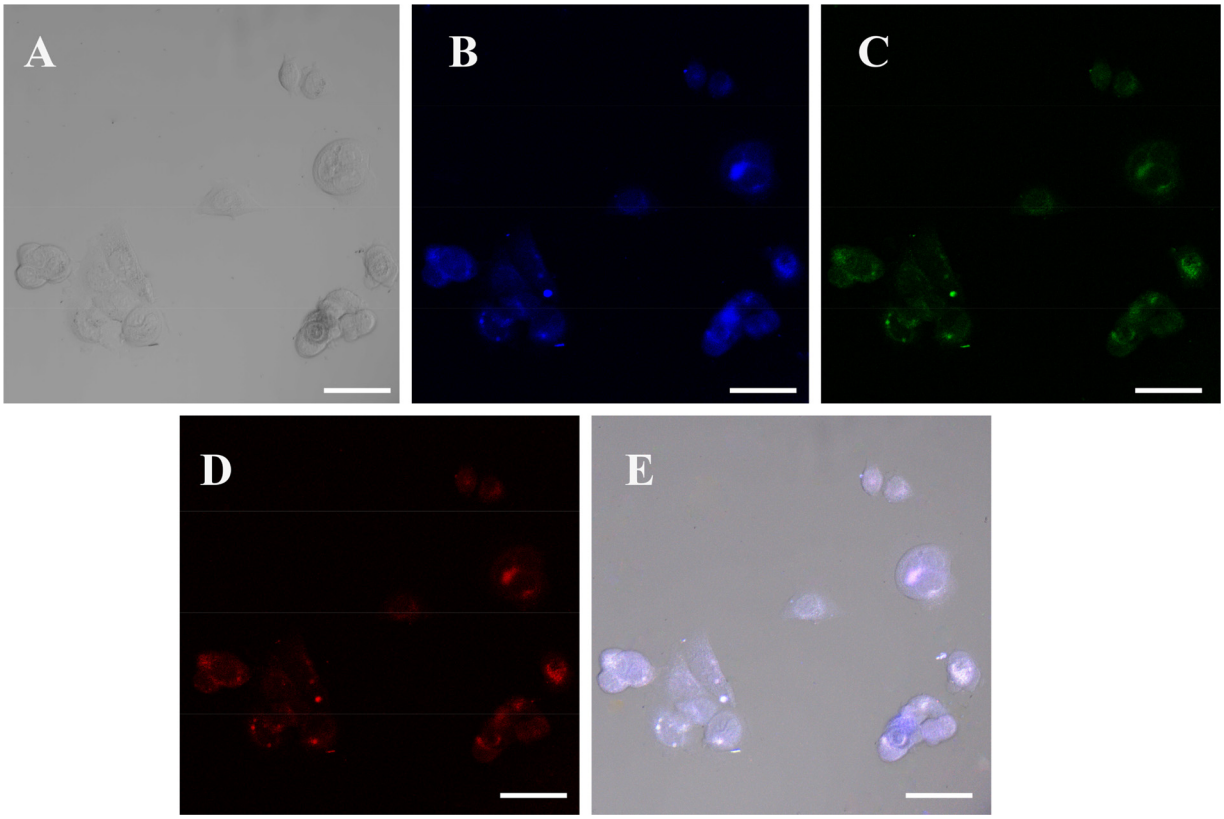

Fig. 4. CLSM images of MCF-7 cells after incubation with CS-1 (100 μg mL^{-1}) for 3 h. A, B, C, D, and E represented the images of bright-field, channel of blue, green, red and overlay, respectively (Scale bar 50 μm).

3.4.2. Bacterial concentration detection and imaging

It is well known that protonated ammonium on chitosan is antibacterial—it can adsorb and accumulate bacteria, penetrate the cell wall, and disturb the metabolism (Kong et al., 2010; Dash et al., 2011). Therefore, utilizing the AIE effect of chitosan and electrostatic interaction with bacteria, the ability of chitosan to detect bacterial concentrations was studied using *E. coli* as a template. The addition of *E. coli* increased the fluorescence intensity of CS-1 (Fig. 5A). As the concentration of *E. coli* increased, the fluorescence of CS-1 gradually increased, because the electrostatic interaction made CS-1 continuously aggregated on the surface of *E. coli*. In the range of 5×10^6 to 5×10^8 CFU mL^{-1}, the ratio I/I_0 of fluorescence intensity changes with (I) and without (I_0) *E. coli* was linear with the bacterial concentration, and the detection limit was 5×10^6 CFU mL^{-1} (Fig. 5B). With good cell imaging capabilities, we further explored the use of chitosan for bacterial imaging. CS-1 was incubated with *E. coli* for 6 h and then CS-1 in the solution was removed by washing with deionized water. Similar to cell imaging, blue, green, and red fluorescence emission were observed in *E. coli* when excited with 405, 488, and 561 nm lasers, respectively (Fig. 6). This promises to achieve real-time multi-channel monitoring of the antibacterial process.

3.4.3. Detection of Fe^{3+}

Fe^{3+} is one of the most important metal ions in living organisms

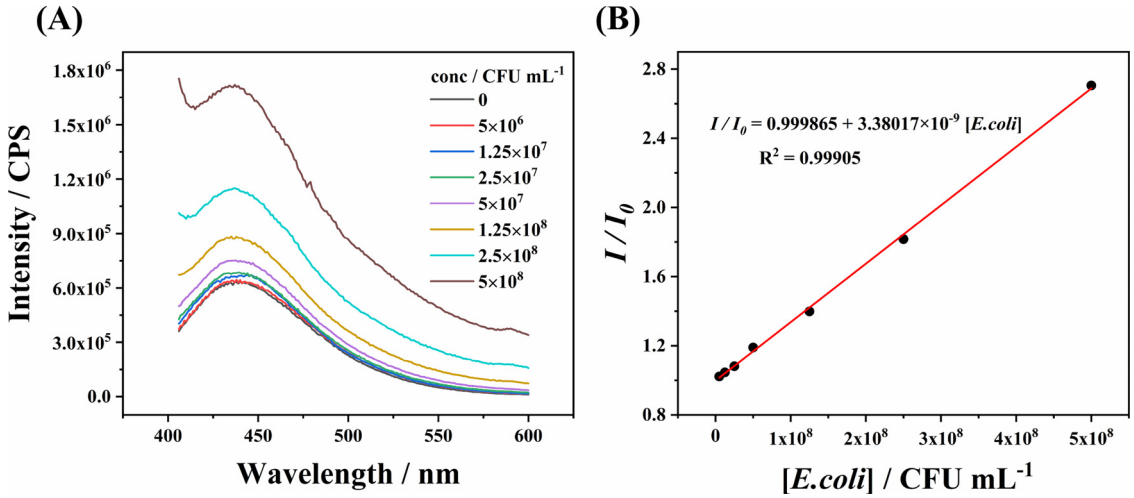

Fig. 5. (A) Fluorescence spectra of CS-1 solution (50 μg mL^{-1}) with the addition of varying concentrations of *E. coli* (slit width: 5 nm). (B) Plots of the I/I_0 at 435 nm against the concentrations of *E. coli* in CS-1 solution.

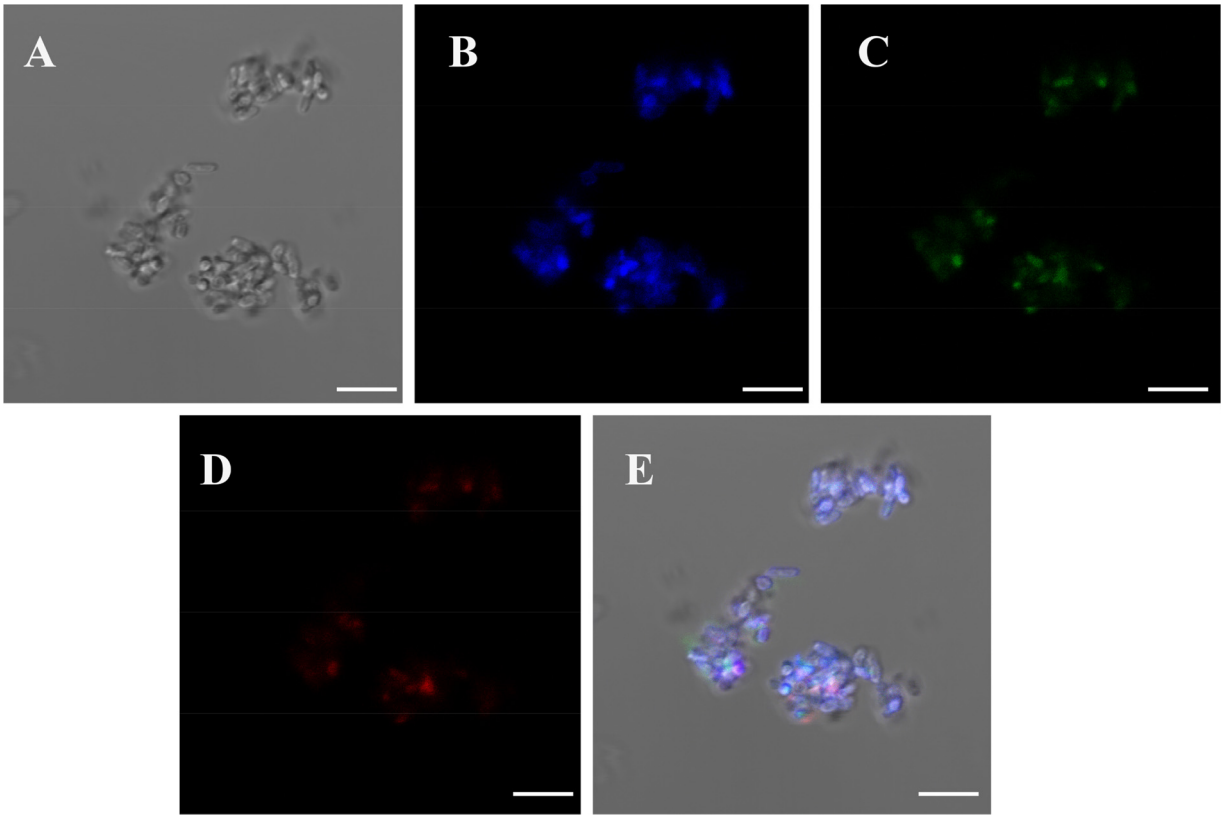

Fig. 6. Confocal laser scanning microscopy images of *E. coli* after incubation with CS-1 (150 μg mL^{-1}) for 6 h. A, B, C, D, and E represented the images of bright-field, channel of blue, green, red and overlay, respectively (Scale bar 5 μm).

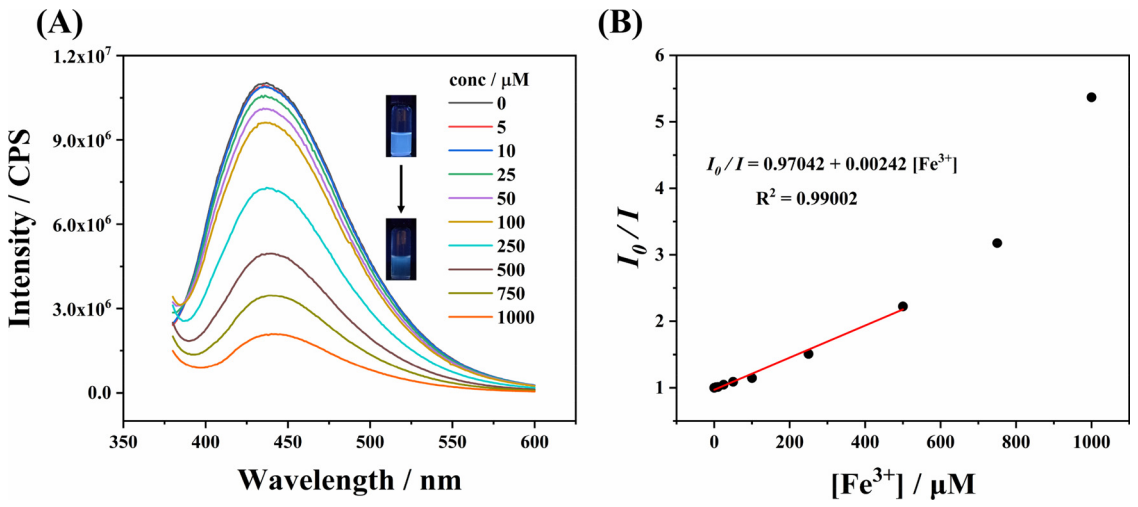

Fig. 7. (A) Fluorescence spectra of CS-1 solution (0.5 mg mL^{-1}) with the addition of varying concentrations of Fe^{3+} (slit width: 5 nm). The inset photographs are the solutions with 0 and 1000 μM Fe^{3+} under 365 nm UV light. (B) Plots of the I/I_0 at 438 nm against the concentrations of Fe^{3+} in CS-1 solution.

(Ananthanarayanan et al., 2014; Li et al., 2014; Zhang & Gan, 2016). Disorders of Fe^{3+} concentration in the human body can induce various diseases. Therefore, the development of a simple, sensitive, safe and reliable Fe^{3+} detection method is of great significance for clinical diagnosis, environmental protection, and industrial production. Fe^{3+} is paramagnetic and has a strong quenching effect on fluorescence (Barba-Bon et al., 2012; Qiu et al., 2014). Therefore, we explored the response of the fluorescence of the CS solution to Fe^{3+}. The fluorescence intensity gradually decreased with continuous addition of Fe^{3+} in CS-1 solution (Fig. 7A). In the range of 5–500 μM, the ratio I_0/I of fluorescence intensity changes with (I) and without (I_0) Fe^{3+} was linear with the Fe^{3+} concentration (Fig. 7B), which satisfied the range of 14–32 μM for the content of Fe^{3+} in normal human serum (Abdolmohammad-Zadeh & Zamani-Kalajahi, 2019). In addition, the response of CS-1 solution to Fe^{3+} was very fast and sensitive. After adding Fe^{3+} to CS-1 solution, the fluorescence intensity decreased rapidly and stabilized within 1 min (**Fig. S12**). These results indicate that the CS solution can detect Fe^{3+} quickly and efficiently. Combined the excellent biocompatibility of CS, it can be used as a biosensor for detecting the concentration of Fe^{3+} in the human body and the environment.

4. Conclusion

In summary, we found the AIE effect of chitosan and verified it by fluorescence spectra. The excellent biocompatibility and AIE effect of CS, motivated the study of its multifunctional applications. Chitosan showed obvious excitation-dependent fluorescence and it could emit a variety of colors from blue to red at different excitation wavelengths and exhibited very excellent multicolor imaging capabilities at the cellular level. On the other hand, *E. coli* can be detected via the AIE effect due to aggregation of CS on the surface of *E. coli*. Concurrently, CS offers good bacterial imaging capabilities, which promises to achieve real-time multi-channel monitoring of the antibacterial process. In addition, the CS solution is capable of detecting Fe^{3+} quickly and efficiently, thus, it can be used as a biosensor for detecting the concentration of Fe^{3+} in the human body and the environment. Therefore, we believe that chitosan as a new class of AIE material will provide a new platform for a variety of practical applications.

Declaration of Competing Interest

There are no conflicts to declare.

Acknowledgment

We are very grateful to the National Natural Science Foundation of China (51671179) for its support.

Appendix A. Supplementary data

Supplementary material related to this article can be found, in the online version, at doi:https://doi.org/10.1016/j.carbpol.2019.115338.

References

Abdolmohammad-Zadeh, H., & Zamani-Kalajahi, M. (2019). A turn-on/off fluorescent sensor based on nano-structured Mg-Al layered double hydroxide intercalated with salicylic acid for monitoring of ferric ion in human serum samples. *Analytica Chimica Acta, 1061*, 152–160.

Ananthanarayanan, A., Wang, X., Routh, P., Sana, B., Lim, S., Kim, D.-H., & Chen, P. (2014). Facile synthesis of graphene quantum dots from 3D graphene and their application for Fe3+Sensing. *Advanced Functional Materials, 24*, 3021–3026.

Barba-Bon, A., Costero, A. M., Gil, S., Parra, M., Soto, J., Martinez-Manez, R., & Sancenon, F. (2012). A new selective fluorogenic probe for trivalent cations. *Chemical Communications, 48*, 3000–3002.

Cao, Q.-Y., Jiang, R., Liu, M., Wan, Q., Xu, D., Tian, J., Huang, H., Wen, Y., Zhang, X., & Wei, Y. (2017a). Microwave-assisted multicomponent reactions for rapid synthesis of AIE-active fluorescent polymeric nanoparticles by post-polymerization method. *Materials Science & Engineering C-Materials for Biological Applications, 80*, 578–583.

Cao, Q.-y., Jiang, R., Liu, M., Wan, Q., Xu, D., Tian, J., Huang, H., Wen, Y., Zhang, X., & Wei, Y. (2017b). Preparation of AIE-active fluorescent polymeric nanoparticles through a catalyst-free thiol-yne click reaction for bioimaging applications. *Materials Science & Engineering C-Materials for Biological Applications, 80*, 411–416.

Chen, X., He, Z., Kausar, F., Chen, G., Zhang, Y., & Yuan, W. Z. (2018). Aggregation-induced dual emission and unusual luminescence beyond excimer emission of poly (ethylene terephthalate). *Macromolecules, 51*, 9035–9042.

Chen, X., Luo, W., Ma, H., Peng, Q., Yuan, W. Z., & Zhang, Y. (2018). Prevalent intrinsic emission from nonaromatic amino acids and poly(amino acids). *Science China-Chemistry, 61*, 351–359.

Chen, Y., Zhang, W., Zhao, Z., Cai, Y., Gong, J., Kwok, R. T. K., Lam, J. W. Y., Sung, H. H. Y., Williams, I. D., & Tang, B. Z. (2018). An Easily Accessible Ionic Aggregation-Induced Emission Luminogen with Hydrogen-Bonding-Switchable Emission and Wash-Free Imaging Ability. *Angewandte Chemie-International Edition, 57*, 5011–5015.

Cheng, Y., Wang, J., Qiu, Z., Zheng, X., Leung, N. L. C., Lam, J. W. Y., & Tang, B. Z. (2017). Multiscale humidity visualization by environmentally sensitive fluorescent molecular rotors. *Advanced Materials, 29*, 1703900.

Dash, M., Chiellini, F., Ottenbrite, R. M., & Chiellini, E. (2011). Chitosan-A versatile semi-synthetic polymer in biomedical applications. *Progress in Polymer Science, 36*, 981–1014.

Dong, Z., Bi, Y., Cui, H., Wang, Y., Wang, C., Li, Y., & Wang, C. (2019). AIE supramolecular assembly with FRET effect for visualizing drug delivery. *ACS Applied Materials & Interfaces, 11*(27), 23840–23847.

Dou, X., Zhou, Q., Chen, X., Tan, Y., He, X., Lu, P., & Yuan, W. Z. (2018). Clustering-triggered emission and persistent room temperature phosphorescence of sodium alginate. *Biomacromolecules, 19*, 2014–2022.

Gu, Y., Zhao, Z., Su, H., Zhang, P., Liu, J., Niu, G., Li, S., Wang, Z., Kwok, R. T. K., Ni, X.-L., Sun, J., Qin, A., Lam, J. W. Y., & Tang, B. Z. (2018). Exploration of biocompatible AIEgens from natural resources. *Chemical Science, 9*, 6497–6502.

Hasan, M. T., Gonzalez-Rodriguez, R., Ryan, C., Faerber, N., Coffer, J. L., & Naumov, A. V. (2018). Photo-and electroluminescence from nitrogen-doped and nitrogen-sulfur codoped graphene quantum dots. *Advanced Functional Materials, 28*, 1804337.

Hou, Z., Shankar, Y. V., Liu, Y., Ding, F., Subramanion, J. L., Ravikumar, V., & Chan-Park, M. B. (2017). Nanoparticles of short cationic peptidopolysaccharide self-assembled by hydrogen bonding with antibacterial effect against multidrug-resistant Bacteria. *ACS Applied Materials & Interfaces, 9*, 38288–38303.

Huang, H., Liu, M., Wan, Q., Jiang, R., Xu, D., Huang, Q., Wen, Y., Deng, F., Zhang, X., & Wei, Y. (2018). Facile fabrication of luminescent hyaluronic acid with aggregation-induced emission through formation of dynamic bonds and their theranostic applications. *Materials Science & Engineering C-Materials for Biological Applications, 91*, 201–207.

Huang, H., Xu, D., Liu, M., Jiang, R., Mao, L., Huang, Q., Wan, Q., Wen, Y., Zhang, X., & Wei, Y. (2017). Direct encapsulation of AIE-active dye with beta cyclodextrin terminated polymers: Self-assembly and biological imaging. *Materials Science & Engineering C-Materials for Biological Applications, 78*, 862–867.

Jiang, M., Gu, X., Kwok, R. T. K., Li, Y., Sung, H. H. Y., Zheng, X., & Tang, B. Z. (2018). Multifunctional AIEgens: Ready synthesis, tunable emission, mechanochromism, mitochondrial, and bacterial imaging. *Advanced Functional Materials, 28*, 1704589.

Jiang, R., Liu, H., Liu, M., Tian, J., Huang, Q., Huang, H., Wen, Y., Cao, Q.-y., Zhang, X., & Wei, Y. (2017). A facile one-pot Mannich reaction for the construction of fluorescent polymeric nanoparticles with aggregation-induced emission feature and their biological imaging. *Materials Science & Engineering C-Materials for Biological Applications, 81*, 416–421.

Kong, M., Chen, X. G., Xing, K., & Park, H. J. (2010). Antimicrobial properties of chitosan and mode of action: A state of the art review. *International Journal of Food Microbiology, 144*, 51–63.

Kumar, M. (2000). A review of chitin and chitosan applications. *Reactive & Functional Polymers, 46*, 1–27.

Kumar, M., Muzzarelli, R. A. A., Muzzarelli, C., Sashiwa, H., & Domb, A. J. (2004). Chitosan chemistry and pharmaceutical perspectives. *Chemical Reviews, 104*, 6017–6084.

Li, M., Long, S., Kang, Y., Guo, L., Wang, J., Fan, J., & Peng, X. (2018). De novo design of phototheranostic sensitizers based on structure-inherent targeting for enhanced Cancer ablation. *Journal of the American Chemical Society, 140*, 15820–15826.

Li, S., Li, Y., Cao, J., Zhu, J., Fan, L., & Li, X. (2014). Sulfur-doped graphene quantum dots as a novel fluorescent probe for highly selective and sensitive detection of Fe3+. *Analytical Chemistry, 86*, 10201–10207.

Liang, J., Tang, B. Z., & Liu, B. (2015). Specific light-up bioprobes based on AIEgen conjugates. *Chemical Society Reviews, 44*, 2798–2811.

Lin, L., Rong, M., Luo, F., Chen, D., Wang, Y., & Chen, X. (2014). Luminescent graphene quantum dots as new fluorescent materials for environmental and biological applications. *Trac-Trends in Analytical Chemistry, 54*, 83–102.

Liu, H., Xie, F., Yu, L., Chen, L., & Li, L. (2009). Thermal processing of starch-based polymers. *Progress in Polymer Science, 34*, 1348–1368.

Liu, Y., Mao, L., Liu, X., Liu, M., Xu, D., Jiang, R., Deng, F., Li, Y., Zhang, X., & Wei, Y. (2017). A facile strategy for fabrication of aggregation-induced emission (AIE) active fluorescent polymeric nanoparticles (FPNs) via post modification of synthetic polymers and their cell imaging. *Materials Science & Engineering C-Materials for Biological Applications, 79*, 590–595.

LogithKumar, R., KeshavNarayan, A., Dhivya, S., Chawla, A., Saravanan, S., & Selvamurugan, N. (2016). A review of chitosan and its derivatives in bone tissue engineering. *Carbohydrate Polymers, 151*, 172–188.

Mei, J., Hong, Y., Lam, J. W. Y., Qin, A., Tang, Y., & Tang, B. Z. (2014). Aggregation-induced emission: The whole is more brilliant than the parts. *Advanced Materials, 26*, 5429–5479.

Mei, J., Leung, N. L. C., Kwok, R. T. K., Lam, J. W. Y., & Tang, B. Z. (2015). Aggregation-Induced Emission: Together We Shine, United We Soar!. *Chemical Reviews, 115*, 11718–11940.

Olsson, R. T., Samir, M. A. S. A., Salazar-Alvarez, G., Belova, L., Strom, V., Berglund, L. A., Ikkala, O., Nogues, J., & Gedde, U. W. (2010). Making flexible magnetic aerogels and stiff magnetic nanopaper using cellulose nanofibrils as templates. *Nature Nanotechnology, 5*, 584–588.

Qin, A., Lam, J. W. Y., & Tang, B. Z. (2012). Luminogenic polymers with aggregation-induced emission characteristics. *Progress in Polymer Science, 37*, 182–209.

Qiu, L., Zhu, C., Chen, H., Hu, M., He, W., & Guo, Z. (2014). A turn-on fluorescent Fe3+ sensor derived from an anthracene-bearing bisdiene macrocycle and its intracellular imaging application. *Chemical Communications, 50*, 4631–4634.

Rinaudo, M. (2006). Chitin and chitosan: Properties and applications. *Progress in Polymer Science, 31*, 603–632.

Shang, C., Wei, N., Zhuo, H., Shao, Y., Zhang, Q., Zhang, Z., & Wang, H. (2017). Highly emissive poly(maleic anhydride-alt-vinyl pyrrolidone) with molecular weight-dependent and excitation-dependent fluorescence. *Journal of Materials Chemistry C, 5*, 8082–8090.

Shen, W., Yu, J., Ge, J., Zhang, R., Cheng, F., Li, X., & Zhu, Q. (2016). Light-up probes based on fluorogens with aggregation-induced emission characteristics for monoamine Oxidase-A activity study in solution and in living cells. *ACS Applied Materials & Interfaces, 8*, 927–935.

Shi, X., Yu, C. Y. Y., Su, H., Kwok, R. T. K., Jiang, M., He, Z., Lam, J. W. Y., & Tang, B. Z. (2017). A red-emissive antibody-AIEgen conjugate for turn-on and wash-free imaging of specific cancer cells. *Chemical Science, 8*, 7014–7024.

Song, F., Xu, Z., Zhang, Q., Zhao, Z., Zhang, H., Zhao, W., & Tang, B. Z. (2018). Highly efficient circularly polarized electroluminescence from aggregation-induced emission luminogens with amplified chirality and delayed fluorescence. *Advanced Functional*

Materials, 28, 1800051.
Song, J., Zhou, H., Gao, R., Zhang, Y., Zhang, H., Zhang, Y., & Zhao, H. (2018). Selective determination of Cr(VI) by glutaraldehyde cross-linked chitosan polymer fluorophores. *ACS Sensors, 3*, 792–798.
Sun, X., Wang, Y., & Lei, Y. (2015). Fluorescence based explosive detection: From mechanisms to sensory materials. *Chemical Society Reviews, 44*, 8019–8061.
Tao, S., Lu, S., Geng, Y., Zhu, S., Redfern, S. A. T., Song, Y., & Yang, B. (2018). Design of metal-free polymer carbon dots: A new class of room-temperature phosphorescent materials. *Angewandte Chemie-International Edition, 57*, 2393–2398.
Tian, G., Sun, D., Zhang, Y., & Yu, X. (2019). Franck-condon blockade and aggregation-modulated conductance in molecular devices using aggregation-induced emission-active molecules. *Angewandte Chemie (International Ed in English), 58*, 5951–5955.
Tian, J., Jiang, R., Gao, P., Xu, D., Mao, L., Zeng, G., Liu, M., Deng, F., Zhang, X., & Wei, Y. (2017). Synthesis and cell imaging applications of amphiphilic AIE-active poly(amino acid)s. *Materials Science & Engineering C-Materials for Biological Applications, 79*, 563–569.
Tian, W., Zhang, J., Yu, J., Wu, J., Nawaz, H., Zhang, J., & Wang, F. (2016). Cellulose-based solid fluorescent materials. *Advanced Optical Materials, 4*, 2044–2050.
Tomalia, D. A., Klajnert-Maculewicz, B., Johnson, K. A. M., Brinkman, H. F., Janaszewska, A., & Hedstrand, D. M. (2019). Non-traditional intrinsic luminescence: Inexplicable blue fluorescence observed for dendrimers, macromolecules and small molecular structures lacking traditional/conventional luminophores. *Progress in Polymer Science, 90*, 35–117.
Wang, D., Su, H., Kwok, R. T. K., Hu, X., Zou, H., Luo, Q., Lee, M. M. S., Xu, W., Lam, J. W. Y., & Tang, B. Z. (2018). Rational design of a water-soluble NIR AIEgen, and its application in ultrafast wash-free cellular imaging and photodynamic cancer cell ablation. *Chemical Science, 9*, 3685–3693.
Wang, K., Yuan, X., Guo, Z., Xu, H., & Chen, Y. (2014). Red emissive cross-linked chitosan and their nanoparticles for imaging the nucleoli of living cells. *Carbohydrate Polymers, 102*, 699–707.
Wang, Z., Chen, S., Lam, J. W. Y., Qin, W., Kwok, R. T. K., Xie, N., & Tang, B. Z. (2013). Long-term fluorescent cellular tracing by the aggregates of AIE bioconjugates. *Journal of the American Chemical Society, 135*, 8238–8245.
Wang, Z., Nie, J., Qin, W., Hu, Q., & Tang, B. Z. (2016). Gelation process visualized by aggregation-induced emission fluorogens. *Nature Communications, 7*, 12033.
Wei, W., Wang, L.-Y., Yuan, L., Wei, Q., Yang, X.-D., Su, Z.-G., & Ma, G.-H. (2007). Preparation and application of novel microspheres possessing autofluorescent properties. *Advanced Functional Materials, 17*, 3153–3158.
Wei, W., Yuan, L., Hu, G., Wang, L.-Y., Wu, H., Hu, X., Su, Z.-G., & Ma, G.-H. (2008). Monodisperse chitosan microspheres with interesting structures for protein drug delivery. *Advanced Materials, 20*, 2292–2296.
Yan, L., Zhang, Y., Xu, B., & Tian, W. (2016). Fluorescent nanoparticles based on AIE fluorogens for bioimaging. *Nanoscale, 8*, 2471–2487.
Yang, W., & Pan, C.-Y. (2009). Synthesis and fluorescent properties of biodegradable hyperbranched poly(amido amine)s. *Macromolecular Rapid Communications, 30*, 2096–2101.
Yang, W., Pan, C.-Y., Liu, X.-Q., & Wang, J. (2011). Multiple functional hyperbranched poly(amido amine) nanoparticles: Synthesis and application in cell imaging. *Biomacromolecules, 12*, 1523–1531.
Yu, Y., Shen, M., Song, Q., & Xie, J. (2018). Biological activities and pharmaceutical applications of polysaccharide from natural resources: A review. *Carbohydrate Polymers, 183*, 91–101.
Zhang, W., & Gan, J. (2016). Synthesis of blue-photoluminescent graphene quantum dots/polystyrenic anion-exchange resin for Fe(III) detection. *Applied Surface Science, 372*, 145–151.
Zhao, J., Dong, Z., Cui, H., Jin, H., & Wang, C. (2018). Nanoengineered peptide-grafted hyperbranched polymers for killing of Bacteria Monitored in real time via intrinsic aggregation-induced emission. *ACS Applied Materials & Interfaces, 10*, 42058–42067.
Zheng, X., Zhu, W., Zhang, C., Zhang, Y., Zhong, C., Li, H., & Yang, C. (2019). Self-assembly of a highly emissive pure organic imine-based stack for electroluminescence and cell imaging. *Journal of the American Chemical Society, 141*, 4704–4710.
Zhu, M., & Yang, C. (2013). Blue fluorescent emitters: Design tactics and applications in organic light-emitting diodes. *Chemical Society Reviews, 42*, 4963–4976.